ANTICANCER RESEARCH *40*: 1875-1882 (2020)
doi:10.21873/anticanres.14141

Detection of Mediastinal Lymph Node Metastases Using Indocyanine Green (ICG) Fluorescence Imaging in an Orthotopic Implantation Model

SHILEI ZHAO[1,2], XIN GUO[3], MAKOTO TANIGUCHI[4], KAZUYA KONDO[5], SOHSUKE YAMADA[3], CHUNDONG GU[1] and HIDETAKA URAMOTO[2]

[1]*Department of Thoracic Surgery, The First Affiliated Hospital of Dalian Medical University, Liaoning, P.R. China;*
[2]*Department of Thoracic Surgery, Kanazawa Medical University, Ishikawa, Japan;*
[3]*Department of Pathology and Laboratory Medicine, Kanazawa Medical University, Ishikawa, Japan;*
[4]*Department of Genome Damage Response Research, Kanazawa Medical University, Ishikawa, Japan;*
[5]*Department of Oncological Medical Services, The University of Tokushima, Tokushima, Japan*

Abstract. *Background: The method of quickly identifying metastatic mediastinal lymph nodes has become an urgent problem for lung cancer surgery. Indocyanine green (ICG) has the characteristic of being retained in or around the lymph nodes; its pharmacokinetic characteristics and optimal imaging time have not yet been elucidated. Materials and Methods: The IVIS Lumina Imaging System was used to detect near infrared (NIR) fluorescence signals at different ICG doses, times and excitation/emission wavelengths in vitro. An artificial lymphogenous metastatic model of squamous lung carcinoma was established in 32 SCID-CB17 mice using Ma44.3 cells. An intratracheal injection of 1.25 ml/kg ICG (1.25×10^{-2} mg/ml) was performed, then 780 nm Ex and 845 nm Em were used to visualize ICG at four different times. The metastatic mediastinal lymph nodes and the implanted local tumor site in the left lung were confirmed with bioluminescence and hematoxylin and eosin (H&E) staining of pathological specimens. Results: ICG had the strongest NIR fluorescence signal when using 780 nm Ex and 845 nm Em at 2 to 4 h after administrating 1.25×10^{-2} mg/ml ICG in vitro. Combined with pathological H&E examination, fluorescence imaging of ICG reflected true-positive mediastinal metastasis of the mediastinum at 0.5 h and 2 h after the injection of ICG in vivo. While true-positive local tumor growth at the site of implantation in the left lung was reflected within 4 h after the injection of ICG. Conclusion: ICG was able to display the metastatic mediastinal lymph nodes within 2 h after endotracheal injection in an orthotopic squamous lung carcinoma implantation model.*

Correspondence to: Chundong Gu, Department of Thoracic Surgery, The First Affiliated Hospital of Dalian Medical University, Zhongshan Road 222#, Dalian 116011, P.R. China. Tel: +86 41183635963 ext. 2061, Fax: +86 41183622844, e-mail: guchundong@dmu.edu.cn and Hidetaka Uramoto, Department of Thoracic Surgery, Kanazawa Medical University, 1-1 Uchinada, Ishikawa 920-0265, Japan. Tel: +81 762862211 ext. 5721, Fax: +81 762861207, e-mail: hidetaka@kanazawa-med.ac.jp

Key Words: Indocyanine green, fluorescence imaging, mediastinal lymphatic metastasis, orthotopic implantation, squamous lung carcinoma.

Pulmonary squamous cell carcinoma (SCC) is an important pathological type of non-small cell lung cancer (NSCLC) and is closely related to smoking (1, 2). SCC mainly occurs in the adjacent hilum area, so it can easily invade vital structures in the mediastinum. In addition, SCC has the characteristics of early lymph node metastasis and is usually diagnosed at an advanced stage (3). Thus, most patients have a poor prognosis and the 5-year survival rate is only 20-30% (4). Surgery, an important treatment method for lung squamous cell carcinoma, is performed to remove the lesion as well as the lymph nodes to eliminate positive or potential lymph node metastasis. Thus, the intraoperative lymph node clearance rate will inevitably determine the patient outcome (5, 6). However, lymph node dissection may result in arrhythmia, injury of the thoracic duct, vessels, esophagus, and trachea, prolonged hospitalization and a reduced quality of life. Hence, lymph node dissection is a double-edged sword. Incomplete dissection may leave residual neoplastic tissue or lead to recurrence. In contrast, extended excision can lead to the excessive exposure of the wound and damage of the adjacent tissues. The development of methods to quickly identify metastatic lymph nodes and realize accurate intraoperative resection has become an urgent issue in clinical practice.

In recent years, near infrared (NIR) spectroscopy has shown unique advantages in optical *in vivo* imaging,

histopathological examination and photodynamic therapy for tumors (7, 8). NIR fluorescent dye has a strong absorption peak (700-900 nm spectral region) and can be stimulated to produce fluorescence. Indocyanine green (ICG), as the only water-soluble NIR fluorescent dye approved for human use by the American Food and Drug Administration (FDA), has been used for imaging of retinal blood vessels and tumors (9-11). In 1986, Matsumura *et al*. proposed that malignant tumor proliferation would induce abnormal neovascularization, so the disordered arrangement among the endotheliocyte in these new vessels with irregular and dilated vascular morphology could allow small molecules to penetrate the vessel walls into intercellular substance followed by lymphatic blockage (12), and the small molecules assemble and arrest in peritumoral or intratumoral lesions. Some subsequent studies (13, 14) found a similar phenomenon wherein ICG as fluorochrome macromolecules continues to accumulate for a long time in tumors due to the retention characteristics of tumor tissues.

Sporadic case reports (15, 16) have shown that when injected around the tumor in chest tumor operations, ICG could accumulate in the intrapulmonary lymph nodes, but not the distant mediastinal lymph nodes. Oh *et al*. (17) reported that the injection of ICG through the segmental bronchus could delay the rate of ICG metabolism and in theory increase its efficiency of lymphatic drainage. Thus, the intratracheal injection of ICG is likely to be an effective method of showing mediastinal lymphatic metastasis. Although this retention gradually weakened with time, it can still be compared with the background of the surrounding normal tissues. Thus, surgeons may accurately identify metastatic lymph nodes intraoperatively through continuous fluorescence-based imaging of ICG.

In the present study, we used a lymphogenous metastatic model of pulmonary squamous cell carcinoma, which was induced in SCID mice *via* surgical orthotopic implantation. After the intratracheal injection of ICG, NIR spectroscopy was performed to explore the dynamic features and optimal imaging time of the primary lesion and mediastinal lymph node metastasis to provide feasible theoretical support for accurate mediastinal lymphadenectomy during surgery.

Materials and Methods

Cell lines and cell cultures. The squamous lung carcinoma cell line (Ma44.3), which was established from the primary lesion of a 68-year-old man with squamous cell lung carcinoma, pT2N0M0, stage IB (18), was kindly gifted by Prof. Kondo and cultured as monolayer in RPMI-1640 medium (GE Healthcare, Chicago, IL, USA) supplemented with 10% fetal bovine serum (GE Healthcare) and maintained in an environment with a humidified incubator under 5% CO_2 at 37˚C.

Surgical orthotopic implantation of primary cultured cancer cells in SCID mice. Thirty-two male SCID mice (CB-17) of 6-8 weeks of age were ordered from CLEA Japan Inc. (Tokyo, Japan) and were maintained in the Laboratory for Animal Experiments. The protocols of all animal experiments were approved by the Institutional Animal Care and Use Committee of the Kanazawa Medical University and were performed according to their guidelines (No: 20-2019). The artificial lymphogenous metastatic model was established according to Ishikura's method (19). The procedure was as follows: The mice were anesthetized by ketamine-medetamidine and placed in the right lateral position, then the skin was incised under the left scapula to dissect the subcutaneous axunge and muscles. When the ribs and intercostal muscles were seen, a microinjection needle (Hamilton Co. Reno, NV, USA) was inserted approximately 5 mm through the intercostal muscles, and primary cultured tumor cells with 10 mg/ml Matrigel (Thermo Fisher Scientific, Waltham, MA, USA) were inoculated at the left lung in a final volume of 10 μl medium (2.0×10^5 cells/ml). Finally, the skin incision was closed with 3-0 silk.

Four (12.5%) of 32 mice orthotopically implanted with Ma44.3 cells died during the modeling process, the remaining mice were randomly divided in equal numbers, into 4 groups according to the different ICG injection times (0.5 h, 2 h, 4 h and 6 h).

In vivo and vitro imaging. Ma44.3 cells (1×10^3) were seeded in 96 wells with 100 μl of complete medium, while control wells only with the same volume of complete medium. The original concentration of ICG (2.5 mg/ml) was diluted at 10^1, 10^2, 10^3, 10^4, 10^5, 10^6, 10^7, 10^8, 10^9 and 10^{10}, then were added in wells and detected at different times (0.25 h, 0.5 h, 1 h, 2 h, 3 h, 4 h, 6 h, 8 h, 12 h, 16 h, 24 h, 48 h and 72 h) and excitation/emission wavelengths (Ex/Em: 680/790, 680/845, 700/790, 700/845, 720/790, 720/845, 740/790, 740/845, 760/845 and 780/845nm) by an IVIS Lumina Imaging System (Caliper Life Sciences, Waltham, MA, USA). The ICG signals of the seeded cells wells and the control wells were quantified with the Living Image 4.0 software program (Caliper Life Sciences) and were represented as the total radiance ($\mu w/cm^2$) and average radiance ($p/sec/cm^2/sr$) (20).

The artificial model of lymphogenous metastasis was anesthetized with ketamine-medetamidine. With the neck fixed and the head tipped back, an incision was made in the middle of the neck, and the submandibular gland and surrounding tracheal tissue were separated. After exposure of the trachea, 1.25 ml/kg ICG (1.25×10^{-2} mg/ml) was injected into the trachea and the skin was closed at the left lateral position. After administration, mice were persistently anesthetized with isoflurane and placed on their dorsal surface, then ICG luciferase signals at 0.5 h, 2 h, 4 h and 6 h using an IVIS Lumina Imaging System (20). Engrafted tumors were illuminated with a 780 nm excitation light, and the NIR fluorescence of ICG was acquired using an 845 nm filter.

Histopathological evaluation. Formalin-fixed, paraffin-embedded, 3-μm-thick sections were obtained from the major organs (bilateral lungs, heart and mediastinal tissues) with hematoxylin and eosin (H&E) for the histopathological diagnosis. All histological slides were evaluated by two independent observers (certified surgical pathologists; X.G. and S.Y.) using a blind protocol design (observers blinded to the clinicopathological data).

Statistical analysis. Data are presented as the mean±standard deviation. Differences between groups were assessed by a two-way analysis of variance or Student's *t*-test. All statistical analyses were

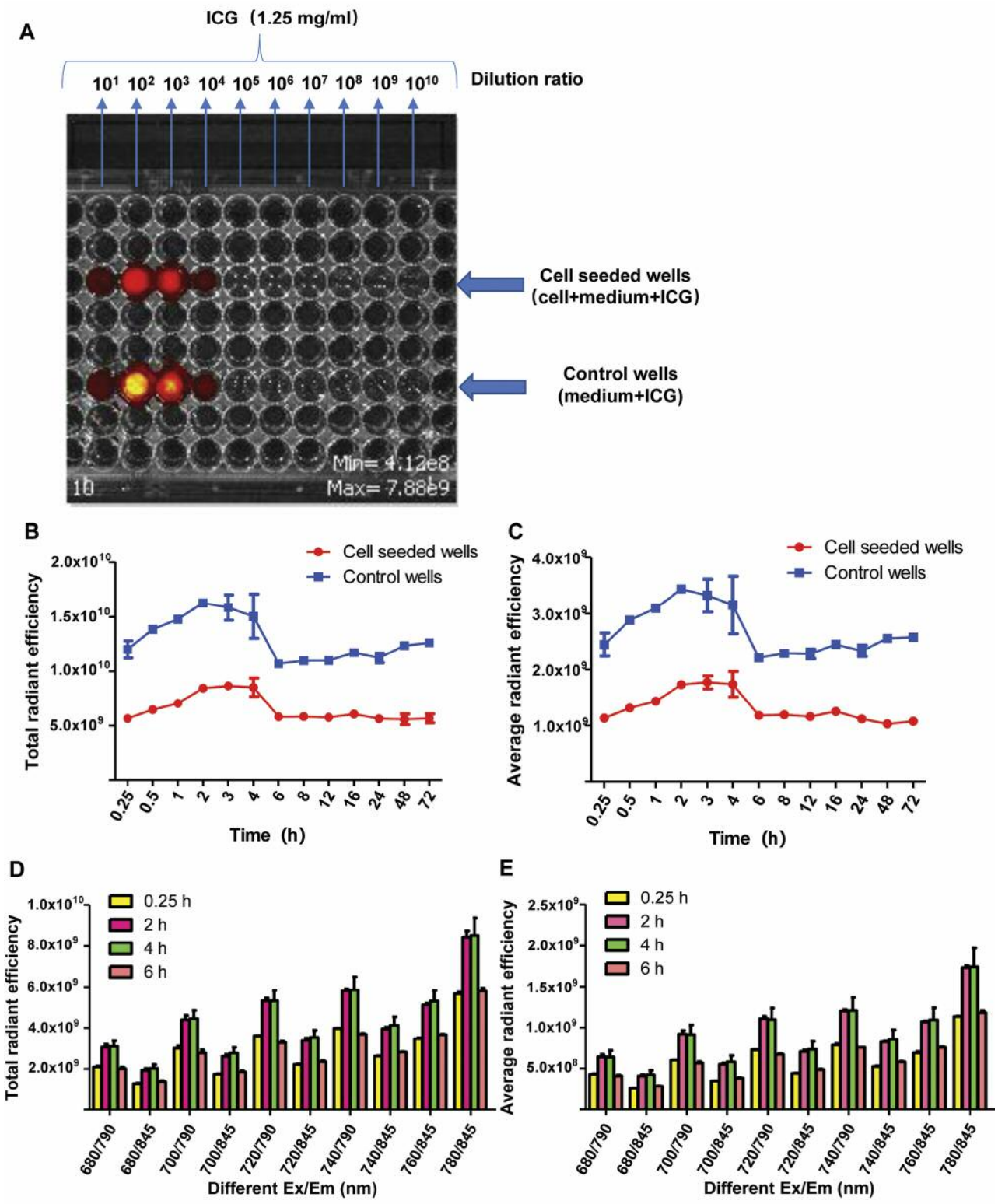

Figure 1. *The change in regularity of ICG in vitro. (A): The change of ICG signal at different concentrations in Ma44.3 cells planked well, and no cells planked well (Control well). The best concentration of the ICG was fixed on 1.25×10^{-2} mg/ml within 72 h. (B and C): The change of ICG signal at different times in Ma44.3 cells planked well and the control well. The ICG (1.25×10^{-2} mg/ml) showed better luminous efficiency (780 nm Ex and 845 nm Em) between 2 h and 4 h. (D and E): The change of ICG signal at different Ex and Em in Ma44.3 cells planked well or and the control well. The ICG (1.25×10^{-2} mg/ml) could reflect the higher radiant efficiency at any time (0.25, 2, 4 or 6 h) when using 780 nm Ex and 845 nm Em.*

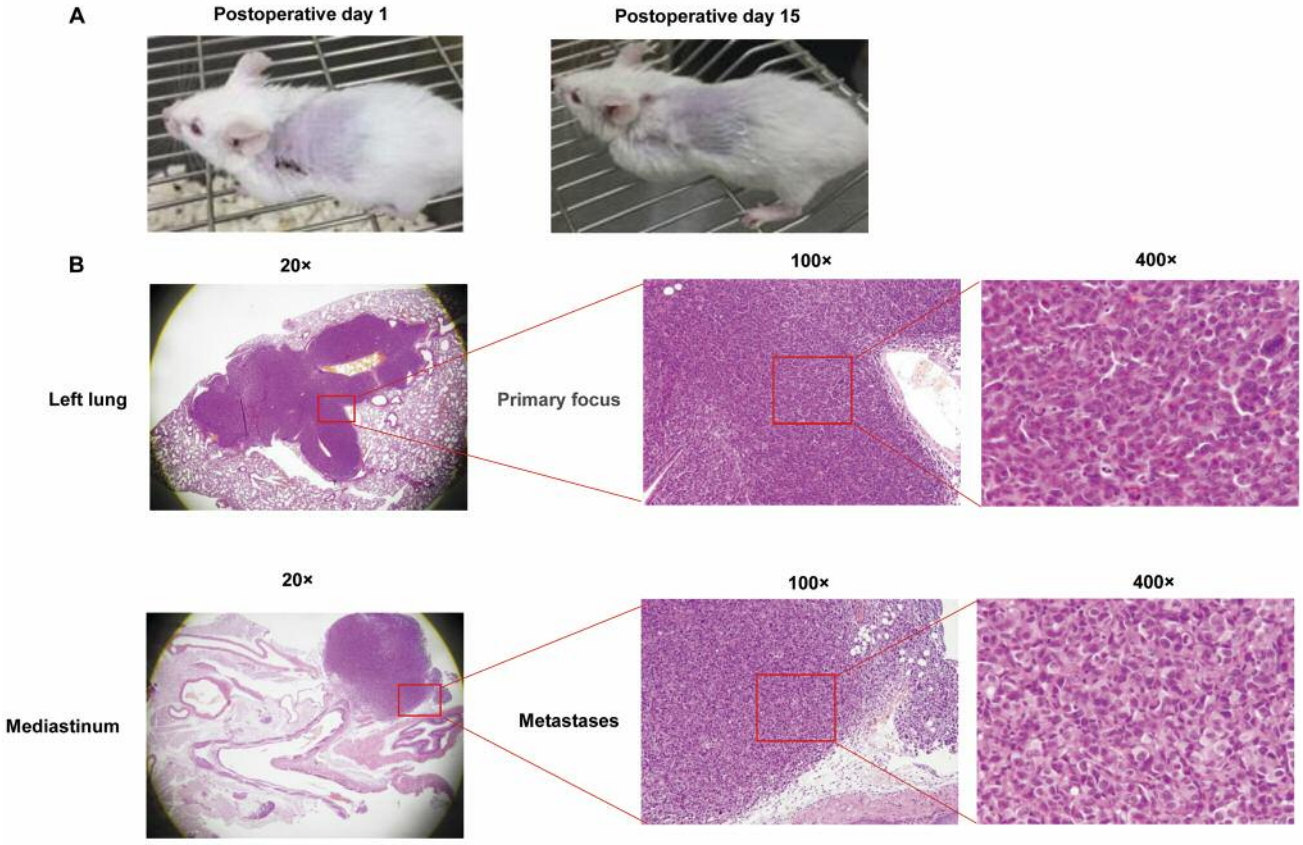

Figure 2. *(A): State of the SCID mouse at postoperative day 1 and 15. (B): Representative H&E staining images of local tumor growth of the implanted site in the left lung and metastases of the mediastinum in mouse orthotopically implanted with Ma44.3 cells at 2 weeks. (Original magnification: ×20; ×100; ×400).*

performed using the SPSS 22 software program (SPSS Inc, Chicago, IL, USA). p-Values<0.05 were considered to indicate statistical significance.

Results

Different doses, times and light excitation of ICG in vitro. NIR fluorescence could only be effectively displayed when the ICG concentration was greater than 1.25×10^{-4} mg/ml. The best concentration of ICG was 1.25×10^{-2} mg/ml within 72 h; in contrast, concentrations of 1.25×10^{-1} mg/ml and 1.25×10^{-4} mg/m were less bright. Figure 1A shows a representative image of ICG signals detected at 2 h using 780 nm Ex and 845 nm Em. When the concentration of ICG was 1.25×10^{-2} mg/ml, the highest total radiant efficiency and average radiant efficiency was observed between 2 and 4 h (Figure 1B and C). In addition, 780 nm Ex and 845 nm Em maximized CG signal (Figure 1D and E).

Tumor formation rate in the orthotopic transplantation metastatic mediastinal tumor model. The state of the mice on postoperative days 1 and 15 is shown in Figure 2A, there was no redness, bleeding or subcutaneous mass in the incision. According to Ishikura *et al*. report (19), the tumor growth was only found in the implanted left lung and mediastinum, but not in the contralateral lung, thymus, liver, kidneys or adrenal glands. Therefore, the bilateral lungs, heart and mediastinal tissues were taken in this study. Metastasis to the mediastinum was observed in all 28 mice (100%), but local tumor growth at the site of implantation in the left lung was only detected in 12 [3, 4, 2 and 3 mice in corresponding group according to the different ICG injection times (0.5 h, 2 h, 4 h and 6 h, respectively)] out of 28 (42.9%) mice at 15 days by H&E staining of pathological specimens (Figure 2B).

Distribution of ICG in tumor in situ (left lung) and ex situ (mediastinum) imaging. All 28 mice survived the intratracheal injection of ICG. Combined with pathological examination, the NIR signal of ICG reflected true-positive metastasis of the mediastinum only at 0.5 h and 2 h after the injection of ICG. At subsequent times, ICG was not useful due to the false-positive results or because the signal was not

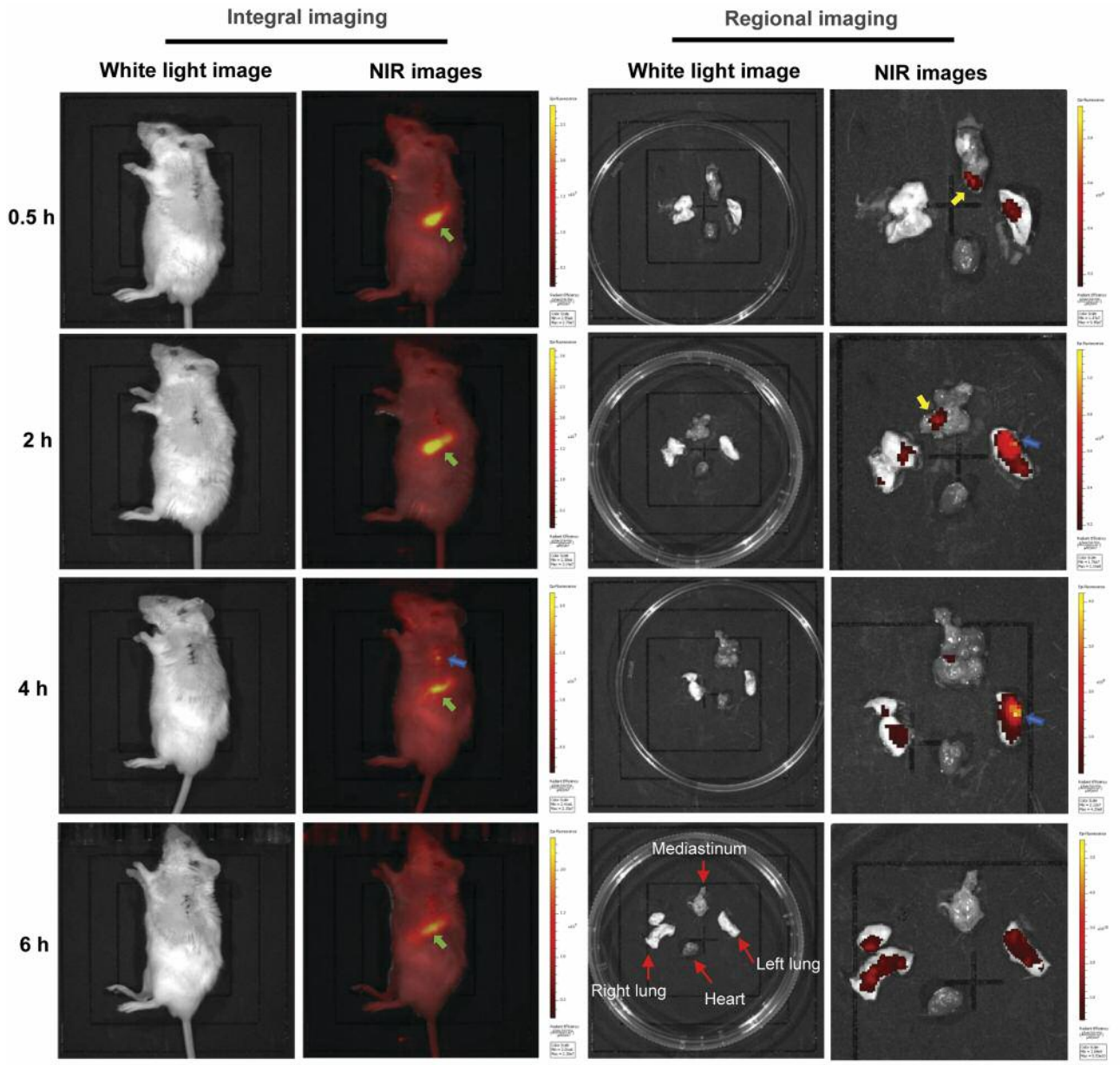

Figure 3. *ICG distribution of the surgical orthotopic transplantation model. near infrared (NIR) imaging of integral and regional organ at 0.5, 2, 4 and 6 h after intratracheal injection of ICG (injected dose: 1.25 ml/kg). The green, blue and yellow arrows point to the developing spleen, primary focus and metastases, respectively.*

detectable (Figure 3). In addition, ICG fluorescence signaling also reflected true-positive local tumor growth at the site of implantation in the left lung at 0.5 h, 2 h and 4 h after intratracheal injection, and the strongest ICG fluorescence appeared at 4 h. However, false-positive results were found in the contralateral lung due to the non-selectivity of tracheal injection (Figure 3). The comparison between ICG imaging and pathological H&E staining at different times is shown in Table I.

Discussion

Many studies (21-23) have shown that different tumors can be well displayed with the intravenous injection of ICG due to pharmacokinetic changes. After the intravenous injection, ICG quickly binds to the plasma protein and is transferred to the liver, then excreted through the biliary system in a prototype form. However, the advantages of continuous imaging have not been reported because of the photobleaching phenomenon

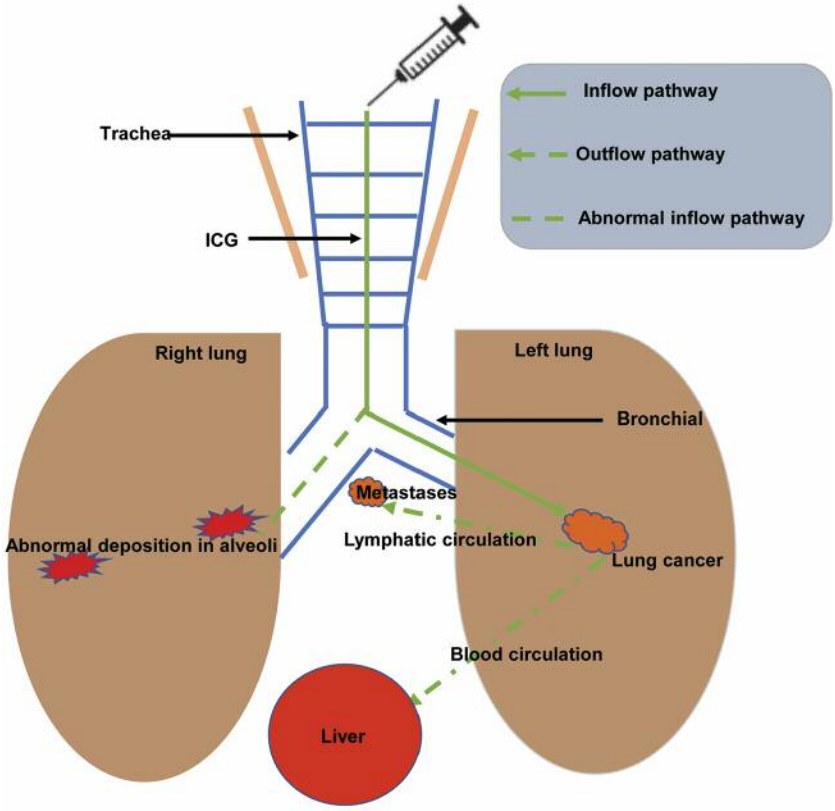

Figure 4. *The dominant flow path of ICG by endotracheal injection.*

Table I. *Comparison between ICG imaging and pathological H&E staining of tumor in the left lung and the mediastinum at different time points.*

ICG Imaging		Tumor in left lung by H&E staining		Tumor in mediastinum by H&E staining	
		(+)	(–)	(+)%	(–)
0.5 h	(+)	1 (33.3%)	2 (50.0%)	1 (14.3%)	0
	(–)	2 (66.7%)	2 (50.0%)	6 (85.7%)	0
2 h	(+)	3 (75.0%)	1 (33.3%)	3 (42.9%)	0
	(–)	1 (25.0%)	2 (66.7%)	4 (57.1%)	0
4 h	(+)	1 (50.0%)	2 (40.0%)	0 (0.0%)	0
	(–)	1 (50.0%)	3 (60.0%)	7 (100.0%)	0
6 h	(+)	0 (0.0%)	3 (75.0%)	0 (0.0%)	0
	(–)	3 (100.0%)	1 (25.0%)	7 (100.0%)	0

and rapid metabolism of ICG *in vivo* (24, 25). It was, therefore, not suitable for persistent imaging of the mediastinal lymph nodes in most lung cancer surgeries. Then, poly-nanoparticle-loaded ICG was designed to overcome these deficiencies. This had a better tumor permeability and aggregation and prolonged the circulation of ICG *in vivo* or caused ICG to be more specifically concentrated in tumor tissues (13, 26). However, the distribution and role of the poly-nanoparticle *in vivo* was still unclear; thus, it has not been applied in clinical practice. Furthermore, metastatic mediastinal lymph nodes in patients with lung cancer were poorly displayed after the intravenous administration of ICG because of the rich adipose tissue surrounding the mediastinal metastases and the lack of necessary nourishing blood vessels (27). In the orthotopic transplantation metastatic mediastinal tumor model, we once attempted to show metastatic mediastinal lymph nodes by intravenously injecting ICG into the tail vein; however, ICG signaling was not deserved in the mediastinal lymph nodes of any of the mice.

Intratracheal injection can delay the excretion of ICG and continuously increase its aggregation in regional lymph nodes due to the passage of lymphatic vessels from structures, such as the interlobular septa and visceral pleura, which have abundant lymphatic capillaries (28). This method, therefore, increases the probability that ICG will accumulate in the mediastinal lymph nodes. In addition, an understanding of the accumulation of ICG in neoplastic tissues *in vivo* could facilitate the intraoperative

arrangement of the ICG injection time to optimize the accumulation of ICG . In this study, accumulation of ICG in left lung primary lesions and mediastinal metastases was visualized by endotracheal injection. We found that ICG could display both pulmonary tumors and mediastinal metastases within 2 h of endotracheal injection. However, the highest sensitivity in ICG imaging of mediastinal metastases was only 37.5%, which is far below the sensitivity of imaging of pulmonary tumors.

We found that ICG had the strongest NIR signal at 780 nm Ex and 845 nm Em after administering the 1.25×10^{-2} mg/ml of ICG for 2 to 4 h *in vitro*, and we hypothesized that the optimal development time of ICG may be shifted to an earlier time and the ICG fluorescence signal may be weakened because of the metabolic dynamics of ICG *in vivo*. However, the optimal imaging time of ICG for primary lung tumor was not longer than that time, this maybe because the tumor induces disorderly and unsystematic neovascularization and the arrest of ICG. The effective detection of ICG in metastatic mediastinal lymph nodes was in line with our hypothesis. Based on the examination of H&E-stained pathological specimens, we could see that the number of peripheral vessels surrounding metastatic mediastinal lesions was significantly lower in comparison to pulmonary lesions; thus, the ICG accumulated at the lymph nodes likely reached the lymph nodes *via* lymphatic circulation. Takizawa *et al*. (16) reported that ICG was imaged through the lymphatic vessels to the sentinel lymph nodes in a patient with lung cancer, which confirmed our results. However, the metabolic mechanism through which ICG reached the metastatic mediastinal lymph nodes remains unclear; thus, further studies were needed (29-32).

The present study is associated with certain limitations (Figure 4). First, there were a few animal deaths in the process of animal modeling, which was inconsistent with the results of Ishikura *et al*. (19). We believe that the difference in mortality was due to individual-animal differences and the large tumor burden in the mediastinum. Second, due to the limitations of experimental techniques, we were unable to inject and limit the ICG solution in the left principal bronchus during the operation, which resulted in the distribution of ICG in the contralateral lung and false-positive imaging of the NIR signal. However, in human lung cancer surgery we can easily complete the injection and restrict ICG to the regional lobar or segmental bronchus, which might reduce false-positive ICG fluorescence in the other lobe.

Conclusion

Endotracheal injection of ICG was able to show the metastatic mediastinal lymph nodes within 2 h in an orthotopic squamous lung carcinoma implantation model.

Conflicts of Interest

The Authors declare that there are no conflicts of interest.

Authors' Contributions

S.Z. participated in its design, experimentation, analysis and manuscript drafting. X.G. and S.Y. mainly performed histopathological examinations. H.U. contributed to theoretical organization of the manuscript. C.G. and H.U. conceived and supervised the study, participated in its design, interpretation, and analysis, including drafting. All Authors contributed to drafting and reviewing the manuscript and approved the submitted and final version.

Acknowledgements

The Authors thank all doctors and staff of the Departments of Pathology and Thoracic Surgery from Kanazawa Medical University for their pathological assistance. This work was supported by Grants-in-Aid for Scientific Research (No:17K10803) from the Ministry of Education, Culture, Sports, Science and Technology, Tokyo, Japan; the National Natural Science Foundation of China (No:81803886, 81774078); the KI.EI.OTO.YO Support Foundation grant from the MSD Life Science Foundation, Astellas Research Support.

References

1 Jamal-Hanjani M, Wilson GA, McGranahan N, Birkbak NJ, Watkins TB, Veeriah S, Shafi S, Johnson DH, Mitter R and Rosenthal R: Tracking the evolution of non–small-cell lung cancer. N Engl J Med *376(22)*: 2109-2121, 2017. PMID: 28445112. DOI: 10.1056/NEJMoa1616288

2 Parascandola M and Xiao L: Tobacco and the lung cancer epidemic in china. Transl Lung Cancer Res *8(Suppl 1)*: S21-S30, 2019. PMID: 31211103. DOI: 10.21037/tlcr.2019.03.12

3 Wistuba II and Gazdar AF: Lung cancer preneoplasia. Annu Rev Pathol Mech Dis *1:* 331-348, 2006. PMID: 18039118. DOI: 10.1146/annurev.pathol.1.110304.100103

4 Skarin AT, Herbst RS, Leong TL, Bailey A and Sugarbaker D: Lung cancer in patients under age 40. Lung Cancer *32(3)*: 255-264, 2001. PMID: 23788919. DOI: 10.5114/wo.2012.31770

5 Tabatabaei SV, Nitche C, Michel M, Rasche K and Hekmat K: Prognostic impact of extracapsular lymph node invasion on survival in non-small-cell lung cancer: A systematic review and meta-analysis. Adv Exp Med Biol *1116*: 27-36, 2018. PMID: 29956198. DOI: 10.1007/5584_2018_238

6 Eichhorn F, Klotz L, Muley T, Kobinger S, Winter H and Eichhorn M: Prognostic relevance of regional lymph-node distribution in patients with n1-positive non-small cell lung cancer: A retrospective single-center analysis. Lung Cancer *138:* 95-101, 2019. PMID: 31678832. DOI: 10.1016/j.lungcan.2019.10.018

7 Zampetti A, Minotto A and Cacialli F: Near-infrared (nir) organic light-emitting diodes (oleds): Challenges and opportunities. Adv Funct Mater *29(21)*: 1807623-1807683, 2019. DOI: 10.1002/adfm.20180762

8 Ning Y, Zhu M and Zhang J-L: Near-infrared (nir) lanthanide molecular probes for bioimaging and biosensing. Coordin Chem Rev *399:* 213028-213047, 2019. DOI: 10.1016/j.ccr.2019.213028

9 Majlesara A, Golriz M, Hafezi M, Saffari A, Stenau E, Maier-Hein L, Müller-Stich BP and Mehrabi A: Indocyanine green fluorescence imaging in hepatobiliary surgery. Photodiagn Photo Dyn *17*: 208-215, 2017. PMID: 28017834. DOI: 10.1016/j.pdpdt.2016.12.005

10 Terasawa M, Ishizawa T, Mise Y, Inoue Y, Ito H, Takahashi Y and Saiura A: Applications of fusion-fluorescence imaging using indocyanine green in laparoscopic hepatectomy. Surg Endosc *31(12)*: 5111-5118, 2017. PMID: 28455774. DOI: 10.1007/s00464-017-5576-z

11 Nakaseko Y, Ishizawa T and Saiura A: Fluorescence-guided surgery for liver tumors. J Surg Oncol *118(2)*: 324-331, 2018. PMID: 30098296. DOI: 10.1002/jso.25128

12 Matsumura Y and Maeda H: A new concept for macromolecular therapeutics in cancer chemotherapy: Mechanism of tumoritropic accumulation of proteins and the antitumor agent smancs. Cancer Res *46*: 6387-6392, 1986. PMID: 2946403.

13 Zhao P, Zheng M, Yue C, Luo Z, Gong P, Gao G, Sheng Z, Zheng C and Cai L: Improving drug accumulation and photothermal efficacy in tumor depending on size of icg loaded lipid-polymer nanoparticles. Biomaterials *35(23)*: 6037-6046, 2014. PMID: 2946403.

14 Kosaka N, Mitsunaga M, Longmire MR, Choyke PL and Kobayashi H: Near infrared fluorescence-guided real-time endoscopic detection of peritoneal ovarian cancer nodules using intravenously injected indocyanine green. Int J Cancer *129(7)*: 1671-1677, 2011. PMID: 21469142. DOI: 10.1002/ijc.26113

15 Nomori H, Cong Y and Sugimura H: Utility and pitfalls of sentinel node identification using indocyanine green during segmentectomy for ct1n0m0 non-small cell lung cancer. Surg Today *46(8)*: 908-913, 2016. PMID: 26350394. DOI: 10.1007/s00595-015-1248-6

16 Takizawa H, Sakiyama S, Tsuboi M and Tangoku A: Demonstration of the skip metastasis pathway for n2 non–small cell lung cancer. J Thorac Cardiovasc Surg *147(4)*: e50-e52, 2014. PMID: 24518224. DOI: 10.1016/j.jtcvs.2013.12.058

17 Oh S, Suzuki K, Miyasaka Y, Matsunaga T, Tsushima Y and Takamochi K: New technique for lung segmentectomy using indocyanine green injection. Ann Thorac Surg *95(6)*: 2188-2190, 2013. PMID: 23706452. DOI: 10.1016/j.athoracsur.2012.12.068

18 Miyoshi T, Kondo K, Ishikura H, Kinoshita H, Matsumori Y and Monden Y: Scid mouse lymphogenous metastatic model of human lung cancer constructed using orthotopic inoculation of cancer cells. Anticancer Res *20(1A)*: 161-163, 2000. PMID: 10769649.

19 Ishikura H, Kondo K, Miyoshi T, Kinoshita H, Hirose T and Monden Y: Artificial lymphogenous metastatic model using orthotopic implantation of human lung cancer. Ann Thorac Surg *69(6)*: 1691-1695, 2000. PMID: 10892908. DOI: 10.1016/s0003-4975(00)01144-9

20 Taniguchi M, Ueda Y, Matsushita M, Nagaya S, Hashizume C, Arai K, Kabayama K, Fukase K, Watanabe K and Wardhani LO: Deficiency of sphingomyelin synthase 2 prolongs survival by the inhibition of lymphoma infiltration through icam-1 reduction. FASEB J, *2020*. PMID: 31970839. DOI: 10.1096/fj.201901783RR

21 Shimada S, Ohtsubo S, Ogasawara K and Kusano M: Macro-and microscopic findings of icg fluorescence in liver tumors. World J Surg Oncol *13(1)*: 198-207, 2015. PMID: 26055754. DOI: 10.1186/s12957-015-0615-5

22 Lieto E, Galizia G, Cardella F, Mabilia A, Basile N, Castellano P, Orditura M and Auricchio A: Indocyanine green fluorescence imaging-guided surgery in primary and metastatic liver tumors. Surg Innov *25(1)*: 62-68, 2018. PMID: 29303061. DOI: 10.1177/1553350617751451

23 Spartalis E, Ntokos G, Georgiou K, Zografos G, Tsourouflis G, Dimitroulis D and Nikiteas NI: Intraoperative indocyanine green (ICG) angiography for the identification of the parathyroid glands: Current evidence and future perspectives. In Vivo *34(1)*: 23-32, 2020. PMID: 31882459. DOI: 10.21873/invivo.11741

24 Otsuka Y and Kaneko H: Usefulness of icg fluorescence imaging in laparoscopic liver resection. *In*: Icg fluorescence imaging and navigation surgery. Kusano M, Kokudo N, Toi M, Kaibori M (eds.). Springer, pp 397-408, 2016.

25 Kengelbach-Weigand A, Lotz L, Schmid R, Lang W, Beckmann MW, Hoffmann I, Horch RE, Renner SP, Dittrich R, Boos AM and Hildebrandt T: Intra-and postoperative blood flow monitoring in a sheep model of uterus transplantation. In Vivo *33(2)*: 325-336, 2019. PMID: 30804109. DOI: 10.21873/invivo.11478

26 Wang H, Li X, Tse BW-C, Yang H, Thorling CA, Liu Y, Touraud M, Chouane JB, Liu X and Roberts MS: Indocyanine green-incorporating nanoparticles for cancer theranostics. Theranostics *8(5)*: 1227-1242, 2018. PMID: 29507616. DOI: 10.7150/thno.22872

27 Uramoto H, Nakajima Y and Kinoshita H: Is the isolated pericardial fat pad sufficient to cover the bronchial stump and separate the pulmonary artery in order to prevent bronchopleural fistula in patients with lung cancer? Anticancer Res *36(5)*: 2385-2389, 2016. PMID: 27127147.

28 van der Pas M, van Dongen G, Cailler F, Pelegrin A and Meijerink W: Sentinel node procedure of the sigmoid using indocyanine green: Feasibility study in a goat model. Surg Endosc *24(9)*: 2182-2187, 2010. PMID: 20177933. DOI: 10.1007/s00464-010-0923-3

29 Breslin JW, Yang Y, Scallan JP, Sweat RS, Adderley SP and Murfee WL: Lymphatic vessel network structure and physiology. Compr Physiol *9(1)*: 207-299, 2011. PMID: 30549020. DOI: 10.1002/cphy.c180015

30 Cousins A, Thompson SK, Wedding AB and Thierry B: Clinical relevance of novel imaging technologies for sentinel lymph node identification and staging. Biotechnol Adv *32(2)*: 269-279, 2014. PMID: 24189095. DOI: 10.1016/j.biotechadv.2013.10.011

31 Farnsworth RH, Achen MG and Stacker SA: The evolving role of lymphatics in cancer metastasis. Curr Opin Immunol *53*: 64-73, 2018. PMID: 29698919. DOI: 10.1016/j.coi.2018.04.008

32 Grigoroiu M Tagett R, Draghici S, Dima S, Nastase A, Florea R, Sorop A, Ilie V, Bacalbasa N, Tica V, Laszlo V, Mansuet-Lupo A, Damotte D, Klepetko W, Popescu I and Regnard JF: Gene-expression profiling in non-small cell lung cancer with invasion of mediastinal lymph nodes for prognosis evaluation. Cancer Genomics Proteomics *12(5)*: 231-242, 2015. PMID: 26417026.

Received February 13, 2020
Revised February 23, 2020
Accepted February 29, 2020